Anomalous Andreev Bound State in Noncentrosymmetric Superconductors

Yukio Tanaka,[1] Yoshihiro Mizuno,[1] Takehito Yokoyama,[2] Keiji Yada,[1] and Masatoshi Sato[3]

[1]*Department of Applied Physics, Nagoya University, Nagoya, 464-8603, Japan*
[2]*Department of Physics, Tokyo Institute of Technology, Tokyo, 152-8551, Japan*
[3]*Institute for Solid State Physics, University of Tokyo, Chiba 277-8581, Japan*

(Received 6 June 2010; published 23 August 2010)

We study edge states of noncentrosymmetric superconductors where spin-singlet d-wave pairing mixes with spin-triplet p (or f)-wave one by spin-orbit coupling. For d_{xy}-wave pairing, the obtained Andreev bound state has an anomalous dispersion as compared to conventional helical edge modes. A unique topologically protected time-reversal invariant Majorana bound state appears at the edge. The charge conductance in the noncentrosymmetric superconductor junctions reflects the anomalous structures of the dispersions, particularly the time-reversal invariant Majorana bound state is manifested as a zero bias conductance peak.

DOI: 10.1103/PhysRevLett.105.097002 PACS numbers: 74.45.+c, 74.20.Rp, 74.50.+r

Recently, physics of noncentrosymmetric superconductors (NCSs) has been one of the important issues in condensed matter physics [1–4]. One of the remarkable features in NCSs is that due to the broken inversion symmetry, superconducting pair potential becomes a mixture of spin-singlet even parity and spin-triplet odd parity [5]. Because of the mixture of spin-singlet and spin-triplet pairings, several novel properties such as the large upper critical field are expected [3,6].

Up to now, there have been several studies about superconducting profiles of NCSs [3,6–13]. In these works, pairing symmetry of NCSs has been mainly assumed to be $s + p$ wave. However, in a strongly correlated system, this assumption is not valid anymore. Microscopic calculations have shown that $d_{x^2-y^2}$-wave spin-singlet pairing mixes with f-wave pairing based on the Hubbard model near half filling [14]. Also, a possible pairing symmetry of superconductivity generated at heterointerface $LaAlO_3/SrTiO_3$ [4] has been studied based on a similar model [15]. It has been found that the gap function consists of spin-singlet d_{xy}-wave component and spin-triplet p-wave one [15]. Therefore, now, it is a challenging issue to reveal novel properties specific to $d_{xy} + p$ or $d_{x^2-y^2} + f$-wave pairing.

The generation of Andreev bound state (ABS) at the surface or interface is a significantly important feature specific to unconventional pairing since ABS directly manifests itself in the tunneling spectroscopy. Actually, for d_{xy}-wave pairing, zero energy dispersionless ABS appears [16]. The presence of ABS has been verified by tunneling experiments of high-T_c cuprate [17] as a zero bias conductance peak (ZBCP). For NCSs, when p-wave pair potential is larger than the s-wave one, it has been shown that ABS is generated at its edge as helical edge modes similar to those in quantum spin Hall system [9–12]. Several new features of spin transport stemming from these helical edge modes have been also predicted [10–13]. However, there has been no theory about ABS in $d_{xy} + p$- or $d_{x^2-y^2} + f$-wave pairing in NCSs. Since tunneling spectroscopy via ABS [16] is a powerful method to identify pairing symmetry and mechanism of unconventional superconductors [17], it is quite important and interesting to clarify ABS and resulting tunneling conductance for $d_{xy} + p$-wave and $d_{x^2-y^2} + f$-wave pairings.

In this Letter, we investigate ABS and tunneling conductance σ_C in normal metal/NCS junctions. For both $d_{xy} + p$-wave and $d_{x^2-y^2} + f$-wave cases, new types of ABS are obtained. In particular, for $d_{xy} + p$-wave case, due to the Fermi surface splitting by spin-orbit coupling, a single branch of topologically stable Majorana bound state appears. Recently, to search for Majorana fermions is one of the hottest issues in condensed matter physics [18,19]. In stark contrast to the other Majorana fermions, the present one preserves time-reversal symmetry. From this difference, the ''time-reversal invariant (TRI) Majorana bound state'' has a peculiar flat dispersion. It shows a unique ZBCP in σ_C depending on the spin-orbit coupling. Therefore, the experimental identification is feasible.

We start with the Hamiltonian of NCS

$$\check{H}_S = \begin{pmatrix} \hat{H}(\mathbf{k}) & \hat{\Delta}(\mathbf{k}) \\ -\hat{\Delta}^*(-\mathbf{k}) & -\hat{H}^*(-\mathbf{k}) \end{pmatrix} \tag{1}$$

with $\hat{H}(\boldsymbol{k}) = \xi_{\boldsymbol{k}} + \boldsymbol{V}(\boldsymbol{k}) \cdot \hat{\boldsymbol{\sigma}}$, $\boldsymbol{V}(\boldsymbol{k}) = \lambda(\hat{\boldsymbol{x}} k_y - \hat{\boldsymbol{y}} k_x)$, $\xi_{\boldsymbol{k}} = \hbar^2 \boldsymbol{k}^2/(2m) - \mu$. Here, μ, m, $\hat{\boldsymbol{\sigma}}$ and λ denote chemical potential, effective mass, Pauli matrices, and coupling constant of Rashba spin-orbit interaction, respectively [3]. The pair potential $\hat{\Delta}(\boldsymbol{k})$ is given by $\hat{\Delta}(\boldsymbol{k}) = [\boldsymbol{d}(\boldsymbol{k}) \cdot \hat{\boldsymbol{\sigma}}] i\hat{\sigma}_y + i\psi(\boldsymbol{k})\hat{\sigma}_y$. Because of the spin-orbit coupling, the spin-triplet component $\boldsymbol{d}(\boldsymbol{k})$ is aligned with the polarization vector of the Rashba spin-orbit coupling, $\boldsymbol{d}(\boldsymbol{k}) || \boldsymbol{V}(\boldsymbol{k})$ [3]. Then, the triplet component is $\boldsymbol{d}(\boldsymbol{k}) = \Delta_t f(\boldsymbol{k})(\hat{\boldsymbol{x}} k_y - \hat{\boldsymbol{y}} k_x)/k$ with $k = \sqrt{\boldsymbol{k}^2}$ while singlet component reads $\psi(\boldsymbol{k}) = \Delta_s f(\boldsymbol{k})$ with $\Delta_t \geq 0$ and $\Delta_s \geq 0$. $f(\boldsymbol{k})$ is given by $f(\boldsymbol{k}) = 2k_x k_y/k^2$ for $d_{xy} + p$ wave and $f(\boldsymbol{k}) = (k_x^2 - k_y^2)/k^2$ for $d_{x^2-y^2} + f$ wave [20]. The superconduct-

ing gaps are $\Delta_1 = |\bar{\Delta}_1(\boldsymbol{k})|$ and $\Delta_2 = |\bar{\Delta}_2(\boldsymbol{k})|$ for the two spin-split band with $\bar{\Delta}_1(\boldsymbol{k}) = (\Delta_t + \Delta_s)f(\boldsymbol{k})$ and $\bar{\Delta}_2(\boldsymbol{k}) = (\Delta_t - \Delta_s)f(\boldsymbol{k})$, respectively, in a homogeneous state [9].

Let us consider a wave function including ABS localized at the surface. Consider a two-dimensional semi-infinite superconductor on $x > 0$ where the surface is located at $x = 0$. The corresponding wave function is given by [11]

$$\Psi_S(x) = [c_1^+ \psi_1^+ \exp(iq_{1x}^+ x) + c_1^- \psi_1^- \exp(-iq_{1x}^- x) + c_2^+ \psi_2^+ \exp(iq_{2x}^+ x) + c_2^- \psi_2^- \exp(-iq_{2x}^- x)] \times \exp(ik_y y), \tag{2}$$

$$q_{1(2)x}^{\pm} = k_{1(2)x}^{\pm} \pm \frac{k_{1(2)}}{k_{1(2)x}^{\pm}} \sqrt{\frac{E^2 - [\bar{\Delta}_{1(2)}(\boldsymbol{k}_{1(2)}^{\pm})]^2}{\lambda^2 + 2\hbar^2\mu/m}},$$

with $k_{1(2)x}^+ = k_{1(2)x}^- = \sqrt{k_{1(2)}^2 - k_y^2}$ for $|k_y| \le k_{1(2)}$ and $k_{1(2)x}^+ = -k_{1(2)x}^- = i\sqrt{k_y^2 - k_{1(2)}^2}$ for $|k_y| > k_{1(2)}$, and $\boldsymbol{k}_{1(2)}^{\pm} = (\pm k_{1(2)x}^{\pm}, k_y)$. Here, k_1 and k_2 are the Fermi wave numbers for the smaller and larger Fermi surface given by $-m\lambda/\hbar^2 + \sqrt{(m\lambda/\hbar^2)^2 + 2m\mu/\hbar^2}$ and $m\lambda/\hbar^2 + \sqrt{(m\lambda/\hbar^2)^2 + 2m\mu/\hbar^2}$, respectively. The wave functions are given by ${}^T\psi_1^{\pm} = (1, -i\alpha_{1\pm}^{-1}, i\alpha_{1\pm}^{-1}\Gamma_{1\pm}, \Gamma_{1\pm})$ and ${}^T\psi_2^{\pm} = (1, i\alpha_{2\pm}^{-1}, i\alpha_{2\pm}^{-1}\Gamma_{2\pm}, -\Gamma_{2\pm})$ with $\Gamma_{1(2)\pm} = \bar{\Delta}_{1(2)}(\boldsymbol{k}_{1(2)}^{\pm})/[E \pm \sqrt{E^2 - [\bar{\Delta}_{1(2)}(\boldsymbol{k}_{1(2)}^{\pm})]^2}]$, and $\alpha_{1(2)\pm} = (\pm k_{1(2)x}^{\pm} - ik_y)/k_{1(2)}$. E is the quasiparticle energy measured from the Fermi energy.

Postulating $\Psi_S(x) = 0$ at $x = 0$, we can determine the ABS. We consider the case for $|k_y| < k_2$. We first focus on the ABS for $d_{xy} + p$-wave case. For $\Delta_t > \Delta_s$, the dispersion ε_b of ABS is given by

$$\varepsilon_b = \begin{cases} \frac{\pm 2\Delta_t \gamma \sqrt{(k_1^2 - k_y^2)(k_2^2 - k_y^2)(k_y^2 - \eta^2 k_1^2)}}{(k_1 + k_2)k_1 k_2} & k_c < |k_y| \le k_1 \\ 0 & k_1 < |k_y| \end{cases} \tag{3}$$

with $\gamma = (k_1/k_2 + k_2/k_1) + (\Delta_s/\Delta_t)(k_2/k_1 - k_1/k_2)$, $\eta = [\Delta_t(1 - k_1/k_2) + \Delta_s(1 + k_1/k_2)]/\{\Delta_t[1 + (k_1/k_2)^2] + \Delta_s[1 - (k_1/k_2)^2]\}$, $k_c = k_1\sqrt{\Delta_t(1 - k_1/k_2) + \Delta_s}/\sqrt{\Delta_t + \Delta_s[1 - (k_1/k_2)^2]}$. On the other hand, for $\Delta_s > \Delta_t$, the resulting ε_b is given by $\varepsilon_b = 0$. The dispersion ε_b of ABS changes drastically at $\Delta_s = \Delta_t$, where one of the energy gaps, i.e., Δ_2, becomes zero. It should be remarked that the present ABSs do not break the time-reversal symmetry.

The resulting ε_b is plotted for various cases in Fig. 1 with $\Delta_0 = \Delta_s + \Delta_t$. For convenience, we introduce dimensionless constant $\beta = 2m\lambda/(\hbar^2 k_f)$ with $k_f = \sqrt{2m\mu/\hbar^2}$. We also plot Δ_1 and Δ_2. Both Δ_1 and Δ_2 become zero at $k_y = 0$. At $|k_y| = k_2$, Δ_2 is always zero. However, Δ_1 then becomes zero only for $\beta = 0$. First, we look at the $\Delta_t > \Delta_s$ case. For $\Delta_s = 0$ with $\beta = 0$, $\varepsilon_b = \pm ck_y$ with some constant c for small k_y [curve a in Fig. 1(a)] as shown in the case of $s + p$-wave pairing [8–13] since $\eta = 0$ is satisfied. This type of ABS is called helical edge mode [11,12,21]. However, this condition is satisfied only for $\Delta_s = 0$ and $\beta = 0$. In fact, ε_b near $k_y = 0$ becomes absent in general as shown in curves a in Figs. 1(b), 1(d), and 1(e). At $k = \pm k_c$, ε_b coincides with $\pm\Delta_2$. For nonzero β, ε_b becomes exactly zero for $|k_y| > k_1$ as shown in curves a in Figs. 1(d) and 1(e). The present line shapes of ε_b are completely different from those of $s + p$-wave superconductors. On the other hand, for $\Delta_s > \Delta_t$, $\varepsilon_b = 0$ for any k_y similar to the case of spin-singlet d_{xy} or spin-triplet p_x-wave pairing [16,17].

We notice here that the zero energy bound state for $|k_y| > k_1$ is a Majorana bound state. The wave function for the zero energy edge state $\Psi_m(k_y)$ can be written as ${}^T\Psi_m(k_y) = (u_1(k_y), u_2(k_y), v_1(k_y), v_2(k_y))$ where

$$u_1(k_y) = -i\sigma v_2(k_y) = \frac{(\alpha f_1 - \beta_1 f_2)\exp(ik_y y - i(\pi/4))}{\sqrt{\sigma\alpha}} \tag{4}$$

$$u_2(k_y) = i\sigma v_1(k_y) = \frac{(f_1 + \beta_2 f_2)\exp(ik_y y - i(\pi/4))}{\sqrt{\sigma\alpha}} \tag{5}$$

with $\alpha = (k_y - \sqrt{k_y^2 - k_1^2})/k_1$, $\beta_1 = (\alpha k_y/k_2 + 1)$, $\beta_2 = (\alpha + k_y/k_2)$, and $\sigma = \mathrm{sgn}(k_y)$. The functions f_1 and f_2 decays exponentially as a function of x and are even function of k_y. The Bogoliubov quasiparticle creation operator for this state is constructed in the usual way as $\gamma^\dagger(k_y) = u_1(k_y)c_\uparrow^\dagger(k_y) + u_2(k_y)c_\downarrow^\dagger(k_y) + v_1(k_y)c_\uparrow(-k_y) + v_2(k_y)c_\downarrow(-k_y)$. Since $u_1(k_y) = v_1^*(-k_y)$ and $u_2(k_y) = v_2^*(-k_y)$ are satisfied, it is possible to verify that $\gamma^\dagger(k_y) = \gamma(-k_y)$. This means the generation of

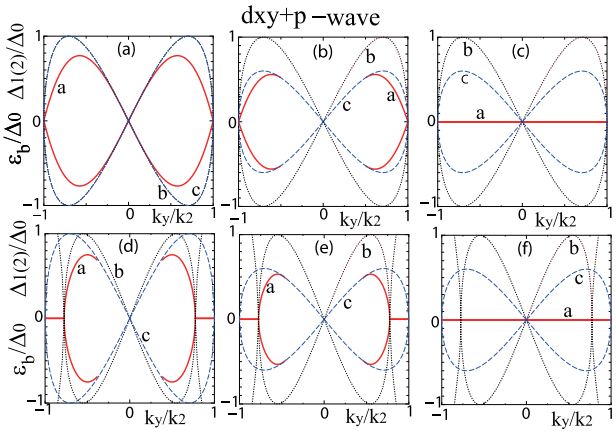

FIG. 1 (color online). Andreev bound state ε_b, effective pair potentials for each Fermi surface Δ_1 and Δ_2 are plotted for the $d_{xy} + p$-wave case as a function of k_y/k_2. $\beta = 0$ for panels (a), (b), and (c). $\beta = 0.5$ for panels (d), (e), and (f). $\Delta_t = \Delta_0$, $\Delta_s = 0$ for (a) and (d). $\Delta_t = 0.8\Delta_0$, $\Delta_s = 0.2\Delta_0$ for (b) and (e). $\Delta_t = 0.2\Delta_0$, $\Delta_s = 0.8\Delta_0$, for (c) and (f). In all panels, curves a (solid line), b (dotted line), and c (dashed line) denote ε_b/Δ_0, Δ_1/Δ_0, and Δ_2/Δ_0, respectively.

Majorana bound state at the edge for $|k_y| > k_1$. For $\Delta_s > \Delta_t$, a similar Majorana bound state also appears for $|k_y| > k_1$. On the other hand, for $|k_y| \leq k_1$, Majorana bound state has double branches and it is reduced to be conventional zero energy ABS.

Unlike Majorana fermions studied before [18,19], the present single Majorana bound state is realized with time-reversal symmetry. The TRI Majorana bound state has the following three characteristics. (a) It has a unique flat dispersion: To be consistent with the time-reversal invariance, the single branch of zero mode should be symmetric under $k_y \rightarrow -k_y$. Therefore, by taking into account the particle-hole symmetry as well, the flat dispersion is required. On the other hand, the conventional time-reversal breaking Majorana bound state has a linear dispersion. (b) The spin-orbit coupling is necessary to obtain the TRI Majorana bound state. Without spin-orbit coupling, the TRI Majorana bound state vanishes. (c) The TRI Majorana bound state is topologically stable under small deformations of the Hamiltonian (1).

We also calculate ABS for the $d_{x^2-y^2} + f$-wave case. In this case, ABS exists only for $\Delta_s < \Delta_t$. In Fig. 2, ε_b is plotted similarly to Fig. 1. As a reference, corresponding ε_b is also shown for the $s + p$-wave case. Helical edge modes around $k_y = 0$ exist and ε_b is absorbed into continuum levels for $|k_y| > k_1$. These features are similar to those of the $s + p$-wave case. However, the number of crossing points of ε_b is five for the $d_{x^2-y^2} + f$-wave case reflecting the complex $\boldsymbol{k}$ dependence of the pair potential. The overall line shapes of ε_b (curve a) in Fig. 2(a) is significantly different from corresponding ε_b (curve a) in Fig. 2(b).

It is very interesting to clarify how the above novel types of ABS are reflected in the charge transport property [9]. The Hamiltonian $\check{H}_N$ in a normal metal is given by putting $\hat{\Delta}(\boldsymbol{k}) = 0$ and $\lambda = 0$ in $\check{H}_S$. We assume an insulating barrier at $x = 0$ expressed by a delta-function potential $U\delta(x)$. The wave function for spin $\gamma = (\uparrow, \downarrow)$ in the normal metal $\Psi_N(x)$ is given by

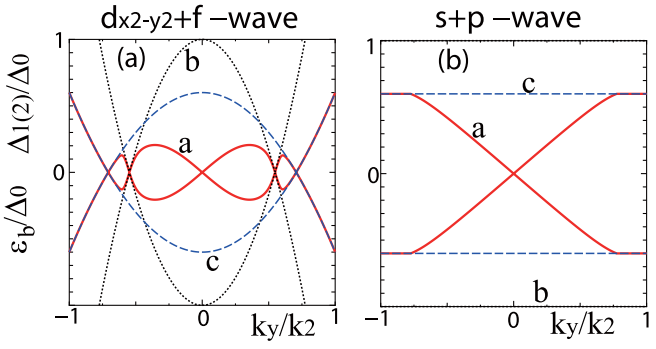

FIG. 2 (color online). Similar plots to Fig. 1 with $\beta = 0.5$ for $d_{x^2-y^2} + f$-wave (a) and $s + p$-wave case (b) with $\Delta_t = 0.8\Delta_0$, $\Delta_s = 0.2\Delta_0$. In all panels, curves a (solid line), b (dotted line), and c (dashed line) denote ε_b/Δ_0, Δ_1/Δ_0, and Δ_2/Δ_0, respectively.

$$\Psi_N(x) = \exp(ik_{Fy}y)\Big[\Big(\psi_{i\gamma} + \sum_{\rho=\uparrow,\downarrow} a_{\gamma,\rho}\psi_{a\rho}\Big)\exp(ik_{Fx}x) + \sum_{\rho=\uparrow,\downarrow} b_{\gamma,\rho}\psi_{b\rho}\exp(-ik_{Fx}x)\Big] \quad (6)$$

with ${}^T\psi_{i\uparrow} = {}^T\psi_{b\uparrow} = (1,0,0,0)$, ${}^T\psi_{i\downarrow} = {}^T\psi_{b\downarrow} = (0,1,0,0)$, ${}^T\psi_{a\uparrow} = (0,0,1,0)$, and ${}^T\psi_{a\downarrow} = (0,0,0,1)$. The corresponding $\Psi_S(x)$ is given by Eq. (2). The coefficients $a_{\gamma,\rho}$ and $b_{\gamma,\rho}$ are determined by the boundary condition $\Psi_N(0) = \Psi_S(0)$, and $\hbar\check{v}_{Sx}\Psi_S(0) - \hbar\check{v}_{Nx}\Psi_N(0) = -2iU\check{\tau}_3\Psi_S(0)$ with $\hbar\check{v}_{S(N)x} = \partial\check{H}_{S(N)}/\partial k_x$, and diagonal matrix $\check{\tau}_3$ given by $\check{\tau}_3 = \mathrm{diag}(1, 1, -1, -1)$.

The quantity of interest is the angle averaged charge conductance σ_C given by

$$\sigma_C = \frac{\int_{-\pi/2}^{\pi/2} f_C(\phi)d\phi}{\int_{-\pi/2}^{\pi/2} f_{NC}(\phi)d\phi}, \quad (7)$$

$$f_C(\phi) = \Big[2 + \sum_{\gamma,\rho}(|a_{\gamma,\rho}|^2 - |b_{\gamma,\rho}|^2)\Big]\frac{\cos\phi}{2}, \quad (8)$$

where $f_{NC}(\phi)$ denotes the angle resolved charge conductance in the normal state with $\hat{\Delta}(\boldsymbol{k}) = 0$. Here, ϕ denotes the injection angle measured from the normal to the interface with $\sin\phi = k_y/k_f$. To characterize transparency of the junction interface, we introduce dimensionless constant $Z = 2mU/\hbar^2 k_f$.

We plot bias voltage $eV = E$ dependence of σ_C for $d_{xy} + p$-wave case in Fig. 3 for various Z. First we concentrate on low transparent junction with $Z = 5$ by changing the value of Δ_s and Δ_t. At $\Delta_t = \Delta_s$, one of the energy gap of the Fermi surface closes corresponding to the quantum phase transition. Then, the resulting σ_C has a gradual change from the quantum critical point. For the case without spin-orbit coupling ($\beta = 0$) with $\Delta_t > \Delta_s$, σ_C has a gap like structure around zero bias due to the absence of Majorana bound state as shown in Figs. 1(a) and 1(b). For $\Delta_s > \Delta_t$, ZBCP appears reflecting the zero energy ABS [17]. In the presence of spin-orbit coupling, σ_C always has a ZBCP independent of the ratio of Δ_s and Δ_t as shown in Fig. 3(b). For $\Delta_t > \Delta_s$, the ZBCP originates from purely TRI Majorana bound state. The width of the ZBCP for $\Delta_t > \Delta_s$ is enhanced with the increase of β, since the region of k_y where the TRI Majorana bound state exists is expanded with β. For $\Delta_s > \Delta_t$, both the conventional ABS and TRI Majorana bound state contribute to the formation of ZBCP. We also plot corresponding σ_C for high ($Z = 1$) and intermediate ($Z = 2$) transparent junctions. For $\Delta_t > \Delta_s$, σ_C has a broad diplike structure around $eV = 0$ for $Z = 1$, while it is slightly enhanced around $eV = 0$ for $Z = 2$ [curves a and b in Figs. 3(c) and 3(d)]. On the other hand, for $\Delta_s > \Delta_t$, σ_C always has a ZBCP [curves d and e in Figs. 3(c) and 3(d)]. The presence of TRI Majorana bound state gives a clear ZBCP with the increase of Z. As a reference, the tunneling conductance σ_C for $d_{x^2-y^2} + f$-wave and $s + p$-wave cases are plotted in

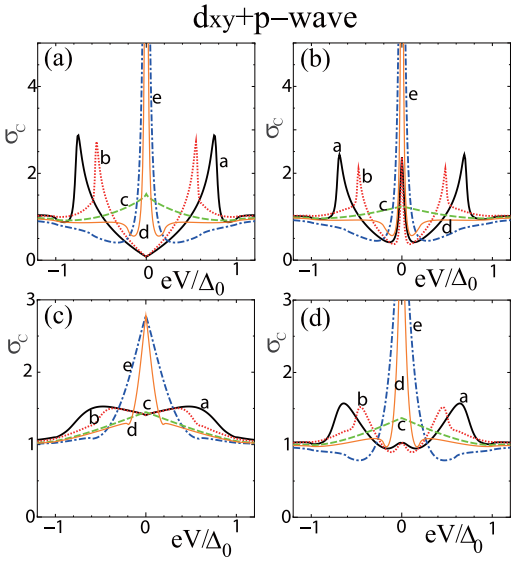

FIG. 3 (color online). Tunneling conductance σ_C for $d_{xy} + p$-wave case. (a) $Z = 5$, $\beta = 0$, (b) $Z = 5$, $\beta = 0.5$, (c) $Z = 1$, $\beta = 0.5$, (d) $Z = 2$, $\beta = 0.5$. *a* (solid line): $\Delta_t = \Delta_0$, $\Delta_s = 0$, *b* (dotted line): $\Delta_t = 0.8\Delta_0$, $\Delta_s = 0.2\Delta_0$, *c* (dashed line): $\Delta_t = 0.5\Delta_0$, $\Delta_s = 0.5\Delta_0$, *d* (thin solid line): $\Delta_t = 0.4\Delta_0$, $\Delta_s = 0.6\Delta_0$, and *e* (dot-dashed line): $\Delta_t = 0.2\Delta_0$, $\Delta_s = 0.8\Delta_0$.

Fig. 4 for $Z = 5$. ABS exists only for $\Delta_s < \Delta_t$. The σ_C for $d_{x^2-y^2} + f$ wave has a ZBCP splitting reflecting the complex dispersion ε_b shown in Fig. 4(a). On the other hand, for $s + p$-wave case, σ_C has a broad ZBCP shown in Fig. 4(b). Summarizing Figs. 3 and 4, σ_C for each paring state are qualitatively different from each other, which can be used to identify these pairings.

In conclusion, we have studied the ABS and resulting charge transport for $d_{xy} + p$-wave and $d_{x^2-y^2} + f$-wave superconductors. We find that the obtained dispersion of ABS in both cases have an anomalous structure. For the $d_{xy} + p$-wave case, a novel TRI Majorana bound state is generated due to the spin-orbit coupling. The resulting charge conductance can serve as a guide to identify the TRI Majorana bound state and paring symmetry of NCSs by tunneling spectroscopy.

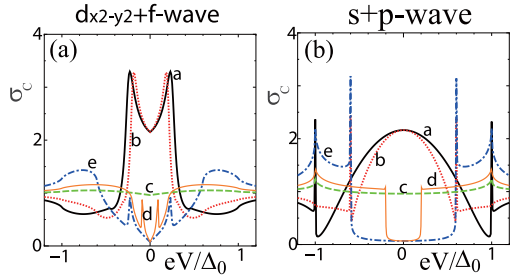

FIG. 4 (color online). Tunneling conductance σ_C with $\beta = 0.5$ and $Z = 5$. (a) $d_{x^2-y^2} + f$ wave and (b) $s + p$ wave. *a* (solid line): $\Delta_t = \Delta_0$, $\Delta_s = 0$, *b* (dotted line): $\Delta_t = 0.8\Delta_0$, $\Delta_s = 0.2\Delta_0$, *c* (dashed line): $\Delta_t = 0.5\Delta_0$, $\Delta_s = 0.5\Delta_0$, *d* (thin solid line): $\Delta_t = 0.4\Delta_0$, $\Delta_s = 0.6\Delta_0$, and *e* (dot-dashed line): $\Delta_t = 0.2\Delta_0$, $\Delta_s = 0.8\Delta_0$.

This work is supported by the Grant-in-Aids for Scientific Research No. 22103005 (Y. T. and M. S.), No. 20654030 (Y. T.), and No. 22540383 (M. S.).

[1] E. Bauer *et al.*, Phys. Rev. Lett. **92**, 027003 (2004).
[2] K. Togano *et al.*, Phys. Rev. Lett. **93**, 247004 (2004); M. Nishiyama, Y. Inada, and G. Q. Zheng, Phys. Rev. B **71**, 220505(R) (2005).
[3] P. A. Frigeri *et al.*, Phys. Rev. Lett. **92**, 097001 (2004).
[4] N. Reyren *et al.*, Science **317**, 1196 (2007).
[5] L. P. Gor'kov and E. I. Rashba, Phys. Rev. Lett. **87**, 037004 (2001).
[6] S. Fujimoto, J. Phys. Soc. Jpn. **76**, 051008 (2007).
[7] Y. Yanase and M. Sigrist, J. Phys. Soc. Jpn. **77**, 124711 (2008); Y. Tada *et al.*, New J. Phys. **11**, 055070 (2009).
[8] J. Linder and A. Sudbø, Phys. Rev. B **76**, 054511 (2007).
[9] T. Yokoyama, Y. Tanaka, and J. Inoue, Phys. Rev. B **72**, 220504(R) (2005); C. Iniotakis *et al.*, Phys. Rev. B **76**, 012501 (2007); M. Eschrig *et al.*, arXiv:1001.2486.
[10] A. B. Vorontsov, I. Vekhter, and M. Eschrig, Phys. Rev. Lett. **101**, 127003 (2008).
[11] Y. Tanaka *et al.*, Phys. Rev. B **79**, 060505(R) (2009).
[12] M. Sato, Phys. Rev. B **73**, 214502 (2006); M. Sato and S. Fujimoto, Phys. Rev. B **79**, 094504 (2009).
[13] C. K. Lu and S. Yip, Phys. Rev. B **80**, 024504 (2009).
[14] T. Yokoyama, S. Onari, and Y. Tanaka, Phys. Rev. B **75**, 172511 (2007); T. Yokoyama *et al.*, J. Phys. Soc. Jpn. **77**, 064711 (2008).
[15] K. Yada *et al.*, Phys. Rev. B **80**, 140509 (2009).
[16] L. J. Buchholtz and G. Zwicknagl, Phys. Rev. B **23**, 5788 (1981); C. R. Hu, Phys. Rev. Lett. **72**, 1526 (1994).
[17] Y. Tanaka and S. Kashiwaya, Phys. Rev. Lett. **74**, 3451 (1995); S. Kashiwaya and Y. Tanaka, Rep. Prog. Phys. **63**, 1641 (2000); A. Biswas *et al.*, Phys. Rev. Lett. **88**, 207004 (2002); B. Chesca *et al.*, Phys. Rev. B **71**, 104504 (2005); **73**, 014529 (2006); B. Chesca, H. J. H. Smilde, and H. Hilgenkamp, Phys. Rev. B **77**, 184510 (2008); M. Wagenknecht *et al.*, Phys. Rev. Lett. **100**, 227001 (2008).
[18] F. Wilczek, Nature Phys. **5**, 614 (2009).
[19] For example, L. Fu and C. L. Kane, Phys. Rev. Lett. **100**, 096407 (2008); M. Sato, Y. Takahashi, and S. Fujimoto, Phys. Rev. Lett. **103**, 020401 (2009); Y. Tanaka, T. Yokoyama, and N. Nagaosa, Phys. Rev. Lett. **103**, 107002 (2009); J. Linder *et al.*, Phys. Rev. Lett. **104**, 067001 (2010).
[20] When the symmetry of the singlet component of pair potential is d_{xy} wave ($d_{x^2-y^2}$ wave), the number of the sign change of the real or imaginary part of triplet one on the Fermi surface is two (six). Thus, we call the mixed pair potential $d_{xy} + p$ wave ($d_{x^2-y^2} + f$ wave).
[21] A. P. Schnyder *et al.*, Phys. Rev. B **78**, 195125 (2008); X. L. Qi *et al.*, Phys. Rev. Lett. **102**, 187001 (2009); R. Roy, arXiv:0803.2868; M. Sato, Phys. Rev. B **79**, 214526 (2009); **81**, 220504(R) (2010).